Food Hydrocolloids xxx (xxxx) xxx

Contents lists available at ScienceDirect

Food Hydrocolloids

journal homepage: www.elsevier.com/locate/foodhyd

Comparison of the molecular structure of heat and pressure-treated corn starch based on experimental data and molecular dynamics simulation

Zhenyu Liu [a,b,c,d], Yongxia Fu [a,b,c,d], Fan Zhang [a,b,c,d], Qingyu Zhao [a,b,c,d], Yong Xue [a,b,c,d], Jinrong Hu [a], Qun Shen [a,b,c,d,*]

[a] College of Food Science and Nutritional Engineering, China Agricultural University, Beijing, 100083, China
[b] National Engineering Research Center for Fruit and Vegetable Processing, Beijing, 100083, China
[c] Key Laboratory of Plant Protein and Grain Processing, Beijing, 100083, China
[d] National Center of Technology Innovation (Deep Processing of Highland Barley) in Food Industry, China

ARTICLE INFO

Keywords:
Corn starch
High hydrostatic pressure
Heating
Gelatinization
Molecular structure
Molecular dynamics

ABSTRACT

The effect of high hydrostatic pressure (HHP) and heating on the molecular structure of corn starch were firstly studied using classical experimental methods and molecular dynamics (MD) simulation. Heat-treated (HT) starches showed more amorphous content further than pressure-treated (PT) starches at similar DGs, further confirming that a higher level of gelatinization occurred after heating. Compared with PT starches, longer external B_2 and B_3 chains (DP > 25) degraded more into A chains (DP 6–12) in HT samples at a similar degree of gelatinization (DG). Heating increased the breakage of α-1,4-glycosidic bonds and significantly reduced molecular weights even one third of the native corn starch at 100% DG. On the other hand, MD results showed that HHP triggered a greater number of amylose-water inter-molecular hydrogen bonds which agreed well with the higher the freedom degree of water molecules in PT starches. Regarding to various energy changes, PT starches exhibited lower bonding-related energies, but higher Van der Waals and electrostatic forces than HT ones. This study adds to understanding of the different molecular features of heating and HHP gelatinization and provides a molecular tool to assist the starch industry in selecting better modification parameters.

1. Introduction

Starch is a cheap and accessible plant component, which acts as the main carbohydrate in the human diet (Rca et al., 2017). Starch has lower solubility in cold water, gel syneresis and poor stability, limiting its application range in its native form (Zhu 2017). These disadvantages are eliminated by modifying native starch with diverse physical, chemical, and enzymatic methods to meet demands for industrial uses (Monroy, Rivero, & García, 2018). In terms of an international report about starch, modified starch will occupy 13.18 billion dollars by 2024 in the global market (Schafranski, Ito, & Lacerda, 2021). Among these modifications, physical modification techniques have become increasingly attractive in recent decades, in pursuit of the aim of reducing potential harm towards consumers and the environment (BeMiller & Huber, 2015). Heating treatment is the most common physical modification, during which an order-disorder phase transition named "gelatinization" occurs (Jacobs & Delcour, 1998, Liu, Wang, Liao, & Shen, 2020). Compared with traditional hydrothermal processing, non-thermal physical processing with high hydrostatic pressure (HHP) as a novel and green modification method can more effectively avoid the degradation of starch and result in less granule swelling and amylose leaching (Pei-Ling, Xiao-Song, & Qun, 2010). Motivated by these features, the application of HHP to gelatinize starch has become a research hotspot.

Various research has evidenced that HHP modification was different from heating on the multi-scale structure and physicochemical properties of starches. For example, at the macroscopic properties level heat and HHP can change the thermal properties, rheological capacities in different ways (Sandhu, Kaur, Punia, & Ahmed, 2021), and texture properties (Larrea-Wachtendorff, Di Nobile, & Ferrari, 2020) of starch. At the micron-sized granule level, heat-treated (HT) starch granules exhibited more disruption with a combination of endo- and exo-corrosion compared with pressure-treated (PT) starches (Liu et al., 2020). Furthermore, at the crystalline structure level, our previous research (Liu et al., 2020) suggested that pressure-gelatinization had a significant impact on both less stable and more stable crystallites, whereas less stable crystallites were preferentially disrupted during heat-gelatinization. At the lamellar structure level, HHP promoted the

* Corresponding author. National Engineering Research Center for Fruit and Vegetable Processing, Beijing, 100083, China.
E-mail address: shenqun@cau.edu.cn (Q. Shen).

https://doi.org/10.1016/j.foodhyd.2021.107371
Received 19 July 2021; Received in revised form 24 September 2021; Accepted 13 November 2021
Available online 17 November 2021

Abbreviations

DSC	Differential scanning calorimeter
HHP	High hydrostatic pressure
HT	Heat-treated
PT	Pressure-treated
DG	Degree of gelatinization
Solid-state ^{13}C CP/MAS NMR	solid-state ^{13}C cross polarization/ magic angle spinning nuclear magnetic resonance
HPAEC-PAD	High-performance anion-exchange chromatography equipped with a pulsed amperometry detector
DP	Degree of polymerization
GPC-MALLS-RI	Gel permeation chromatography assisted with multiangle laser-light scattering detector and refractive index detector
M_w	Weight-average molecular mass
R_z	Z-average radius of gyration
LF-NMR	Low field nuclear magnetic resonance
T_2	Transverse relaxation time
MD	Molecular dynamics
VDW	Van der Waals

growth of the transition layer, and maize starch (0.3 nm) showed more obvious change than quinoa starch (0.1 nm) (Li, Zhu, Mo, & Hemar, 2019). However, it is believed that even lower levels of starch structure, such as helical and molecular structure, play essential roles in determining higher level starch structure (Takeda, Takeda, Mizukami, & Hanashiro, 1999; Yu et al., 2020), and thus gelatinization processing (Li & Gong, 2020). Hence, in the present work, the comparative study on the molecular structure of heat and pressure-treated corn starch at similar degree of gelatinization (DG) was needed to better understand basic HHP gelatinization mechanisms deduced by the molecular structure changes.

Furthermore, molecular dynamics (MD), as a promising method, can simulate the interaction of molecules over a specific time period under the influence of the laws of physics, including quantum and classical mechanics theories (Feng et al., 2015). It is considered to provide a direct insight towards the molecular interaction and energy state of the polymer-based systems, which recently has been employed to establish and model the starch-based complexes (Cheng et al., 2018; Chen et al. 2020). Cui et al. studied the changes in hydrogen bonds interaction and the distribution of starch fragments in the presence of urea and water using MD combined with traditional characterization methods (Cui, Zi, Liu, Zhang, & Yuan, 2020). Owning to inaccuracy and limitations of existing experimental approaches to explore the molecular interactions and configurations between starch and water molecular on atomic scale, MD has been employed to study the detailed characteristics of amylose-water systems under various heating and HHP conditions. Gelatinization of starch granules is a vital and complex process, and the mechanisms of heat and HHP gelatinization at the molecular level are unclear and a matter of much debate, such as why heat and HHP treatment causes similar change trends but the degree of change differs for multi-scale structural features (Liu et al., 2020). This lack of information hinders further understanding of starch structure-function relationships. The objectives of the present study were to explore (i) the effect of heating and HHP on the molecular structure of corn starch at similar DG with traditional characterization methods, (ii) the molecular interactions and energy states of amylose-water systems after heating and pressurizing via MD, and (iii) the mechanisms of heating and pressure gelatinization deduced by the molecular structure changes. It would be helpful to reveal the molecular mechanism of heating and HHP gelatinization and give a new perspective on the correlation between molecular structure changes and intermolecular and intramolecular interactions of starch-water system.

2. Experimental section

2.1. Materials and sample preparation

The corn starch was isolated from corn kernel (cultivar: Qiangsheng 62) donated by the China Grain Reserves Corporation following the method of (Liu et al., 2020). Its average composition was 91.08% carbohydrate, 8.18% moisture, 0.23% ash, 0.51% crude protein and lipid (undetected). All the chemical reagents used in this study were of analytical grade.

2.2. Heat and HHP treatment of corn starch

The slurries were made by suspending native corn starch in distilled water with a concentration of 20 wt%. The HT and PT corn starches were prepared in the same way referring to our previous paper which were presented as below (Liu et al., 2020). (1) The HHP treatments were conducted under 400–600 MPa for 10–20 min by a high static pressure press (type HPP-1700-2; KeFa High- Pressure Technology Co., Ltd., Baotou, China). During the HHP experiments, the pressure boost procedure would not exceed 2 min, and the depressurization time would be less than 2 s, respectively. The initial temperature of PT corn starches was around 25 °C. The maximum temperature of each PT corn starches was not over 35 °C, which was below the heat gelatinization temperature. (2) The heating treatments were conducted in a glass vessel with constant stirring at 65–75 °C for 10–20 min by digital heating circulating water bath. Afterward, the treated corn starch suspension was frozen at −80 °C and freeze-dried. The dried powder was pulverized using an electric beater and sifted through a 100-mesh sieve. The obtained powder was placed in sealing bag and stored in a desiccator until further analysis.

2.3. DSC analysis

The DG of the HT and PT corn starches was measured by DSC-60 (Shimadzu Corporation, Japan). 3 mg of native or treated corn starch suspension and 12 μL distilled water were sealed in a standard aluminum pan (AL-HERMETIC, S201-53090), and an empty pan was performed as a reference. Tests were performed in triplicate in a temperature range of 30–100 °C with a heating rate of 10 °C/min. The melting enthalpy (ΔH) associated with starch gelatinization was obtained from the area of the peak endotherm as described by (Zhong & Sun, 2005) and values for the DG were calculated as:

$$DG\% = \frac{\Delta H_{ns} - \Delta H_{ts}}{\Delta H_{ns}} \times 100\%$$

where ΔH_{ns} and ΔH_{ts} referred to the melting enthalpies of native and modified corn starches, respectively.

Five various DGs were achieved under heating and HHP treatment, including that DG1was approximately 20% which corresponded to 65 °C/10 min and 400 MPa/10 min, DG2 was approximately 50% which corresponded to 70 °C/10 min and 500 MPa/10 min, DG3 was approximately 70% which corresponded to 73 °C/10 min and 550 MPa/10 min, DG4 was approximately 85% which corresponded to 75 °C/10 min and 600 MPa/10 min, DG5 was approximately 100% which corresponded to 75 °C/20 min and 600 MPa/20 min.

2.4. ^{13}C CP/MAS NMR analysis and Peak-Fitting procedure

Solid-state ^{13}C NMR measurements were determined using a Bruker AVIII-400 spectrometer equipped with a 4 mm CP/MAS detection probe (Bruker Co. Ltd., Germany). The spectra were acquired using a ^{13}C

frequency of 104.29 MHz and a spectral width of 50 kHz 200 mg dry and sieving samples were packed in a 4 mm ZrO2 rotor sealed with a Kel-F cap and spun at the magic angle (54.7°) with 12 kHz of spin rate. Tests were performed at a contact time of 2 ms and a total of 10,240 scans were recorded with a recovery period of 5 s per sample. All ^{13}C CP/MAS chemical shifts were referenced to the resonance of adamantane ($C_{10}H_{16}$) standard (δCH2 = 38.4). The areas of the amorphous and ordered subspectra relative to the total area of the spectrum at the C_1 region yielded the proportion of amorphous and ordered components. The spectra were peak fitted by using PeakFit 4.12 (Jandel Scientific Software, CA). Finally, the proportions of double and single helical structures and amorphous phase in the starch samples were calculated according to the method described by Tan (Tan, Flanagan, Halley, Whittaker, & Gidley, 2007).

2.5. Branch chain-length distribution of amylopectin using HPAEC-PAD

The chain length distribution was acquired according to the method of (Li, Oh, Lee, Baik, & Chung, 2017) with some modifications. Briefly, precisely 5 mg of each sample was heated in a boiling water-bath with occasional stirring for 60 min, and then 2.5 mL of gelatinized sample was added to a mixture of 125 μL sodium acetate buffer and 5 μL NaN_3. After cooling to room temperatre, 5 μL of isoamylase was added and incubated in a shaking water bath (100 r/min) at 37 °C for 24 h. Aliquots of 600 μL were placed in centrifuge tubes and dried with nitrogen at room temperature. The samples were dissolved in 600 μL mobile phase and centrifuged at 12,000 rpm for 5 min. Approximately 20 μL of supernatant were injected into a high-performance anion-exchange chromatography (HPAEC) system (ICS500+, Thermo Fisher Scientific, USA) equipped with a pulsed amperometry detector (PAD) at 30 °C and assisted with a chromatographic column (Dionex™ CarboPac™ PA10).

2.6. Molecular weight analysis using GPC-MALLS-IR

Molecular weight distributions were measured following a method (Al-Ansi et al., 2021) with some modifications. Briefly, approximately 5 mg of corn starch was dissolved in 1 mL of 99.5 wt% dimethyl sulfoxide (DMSO) and 0.5 wt% lithium bromide (LiBr) solution and placed in a hot water bath at 60 °C for 24 h with continuous stirring. Samples were centrifuged at 14000 rpm for 10 min and then 300 mL of supernatant were injected into a GPC instrument (U3000, Thermo, USA) equipped with a multiangle laser-light scattering (MALLS) and refractive index detectors (Wyatt Technology, CA 93, USA) and two organic SEC columns Ohpak SB-805 HQ (300 × 8 mm). The temperature was maintained at 65 °C for all columns. The eluent was 99.5 wt% DMSO and 0.5 wt% LiBr solution at a flow rate of 0.4 mL/min.

2.7. ^1H nuclear magnetic resonance (NMR) spectroscopy

The ^1H NMR spectra was obtained by a Bruker Avance II 600 MHz spectrometer at the Center for Nuclear Magnetic Resonance, Tsinghua University. Prior to testing, 10 mg starch sample was completely dissolved in 1 mL DMSO-d_6 heating at 40 °C for 1.5 h. Each mixture was transferred to a 5 mm NMR tube and tightly sealed before an NMR spectrum was recorded. And then the NMR data were measured for 16 scans at 25 °C. The chemical shift scale was calibrated using the residual DMSO-d_6 signal at 2.549 ppm. Finally, the analysis was carried out on Delta 5.3.1 software.

2.8. Measurements of the transverse relaxation time (T_2) by LF-NMR

The relaxation time was collected using a LF-NMR spectrometer (Niumag Electric Corporation, Shanghai, China), operated at a proton resonance frequency of 21.96 MHz and a magnetic field strength of 0.52 T. The samples were balanced in a 10 mm LF-NMR tube sealed with film to prevent moisture loss. Firstly, turn on the nuclear magnetic instrument and preheat the magnet for 24 h and keep the temperature of the magnet constant at 32 °C. The standard soybean oil sample was used for instrument calibration. The magnetic field was homogenized and the instrument center frequency and instrument 90° pulse width of hard pulse were determined. Afterward, the exact mass 0.8 g of the sample in each tube was tested using the multi-pulse echo sequence named CPMG. The experimental parameters were set according to (Fan et al., 2013) with a slight modification. The pulse width was set to 90° and 180°, with a 90° pulse time of 2.6 μs and a 180° pulse time of 5.12 μs. For the CPMG test, the half-echo time was 60 μs, the echo number was 1000, the cumulative number of scans was 128, the repeat time between two scans was 300 ms, the analog gain was 20, and the digital gain was three.

2.9. Molecular dynamics simulation

MD simulations and analysis were carried out using GROMACS, 2018.3 (H., Berendsen et al., 1995, Spoel, Lindahl, Hess, Groenhof, & Berendsen, 2005; Mja et al., 2015). Normally, simple models are used to operate MD simulations. Cheng et al. (Cheng et al., 2018) used a V-type helix with 26 residues as the initial model. Based on this, a left-helix and V-type helix amylose model consisting of 25 glucose residues was constructed in this study. The different temperature conditions of HT gelatinization were set at: 65 °C, 70 °C, 75 °C, and the various pressure conditions of PT gelatinization were set at: 400 MPa, 500 MPa, 600 MPa, with three parallel simulations of each simulation. Every simulation was performed using glycam 06 and tip3p force fields (Price & Brooks, 2004, Lu, Qiu, Baron, & Molinero, 2014). A leap-frog scheme, periodic boundary conditions and an appropriate 1.2 nm cutoff distance were used in the simulation process. All MD simulations were performed in an isothermal and isobaric ensemble with temperature and pressure controlled by the V-Resale and Parrinello-Rahman methods, respectively, with coupling constants of 0.1 and 0.5 ps. Simulation files were extracted every 0.01 ns to calculate the numbers of inter-, intra-molecular hydrogen bonds and energies. The presence of a hydrogen bond was determined by the criteria in which the maximum distance between the donor and acceptor atoms is 0.35 nm (Zhi-guang et al., 2020). The total simulation time was 100 ns.

2.10. Statistical analysis

All experiments were performed in triplicate and the data were expressed as mean ± standard deviation. Graphs were constructed in Origin 2018 (OriginLab Corporation, Northampton, MA). Statistical data analysis was carried out using IBM-SPSS-25 software (SPSS Inc., Chicago, USA) ($p < 0.05$). An independent two sample T-test between HT and PT starch under similar DG was also performed.

3. Results and discussion

3.1. Helical conformation

Solid state ^{13}C CP/MAS NMR has been used to quantify the arrangement of HT and PT corn starch chains. As shown in Fig. 1, the ^{13}C CP/MAS NMR spectra of HT and PT corn starch are presented. There exists six partially overlapping lines which represents the chemical shifts of carbons in the starch. The resonance at 58–68 ppm is assigned to C_6 and the overlapping signal around 68–79 ppm is collectively associated with the C_2, C_3, and C_5 sites. The signal intensities around 80–84 ppm and 90–110 ppm are related to the C_4 and C_1 sites, respectively, which is consistent to a previous report (Tan et al., 2007). As revealed by the ^{13}C NMR patterns, distinct triplet peaks (with 100.1, 101.2, and 101.9 ppm) were observed in the C_1 signal region of native corn starch which were found to be a sensitive indicator of the variations of A-type helical conformation (Fig. 1). The intensity of the triplet peaks in HT and PT starches showed weaker with increasing DG, and even for HT4, HT5 and PT5 starches, the triplet peaks became only a broad resonance at 103

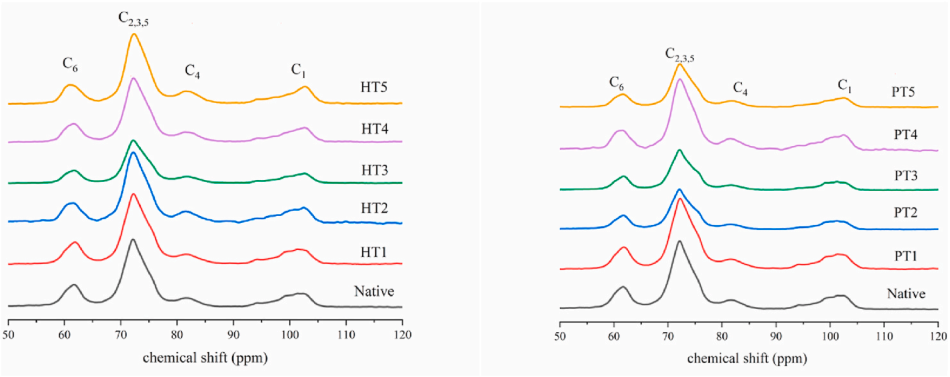

Fig. 1. ^{13}C CP/MAS NMR spectra of HT and PT corn starch at different approximate DGs (HT1 and PT1, 20% DG; HT2 and PT2 50% DG; HT3 and PT3 70% DG; HT4 and PT4, 85% DG; HT5 and PT5, 100% DG).

ppm which corresponds to the distortion of crystal structure under heating and pressurization. The two characteristic peaks near 103 ppm in the C_1 region and 82 ppm in the C_4 region provides information about the amorphous and ordered components in corn starch (Paris, Bizot, Emery, Buzaré, & Buléon, 1999). Decomposition of the spectrum into sub-spectra related to phase composition is shown in Supplementary Fig. 1, including the proportion of the amorphous and ordered phase. For HT and PT starches, the signal representing the amorphous state gradually intensified. Moreover, HT starches showed more amorphous content further than PT starches at similar DGs, further confirming that a higher level of gelatinization occurred after heating. Referring to DSC results shown in Supplementary Table 1, it was reasonable that narrower gelatinization temperature range in HT starch occurred than that of PT one at a similar DG.

It is worth noting that the helical structure of starches can be used to interpret various process-induced changes. According to calculations based on the deconvolution by PeakFit 4.12, the relative proportion of double-helix and single-helix components gradually decreased and the amorphous content correspondingly increased with increasing DG in HT and PT starches (Table 1), indicating that heating and pressure contributed to degradation of the intermolecular hydrogen bonding within starches. The double helix and single helix might be converted into the amorphous phase either directly or dissociated into single chains (Šoltýs et al., 2019). For HT (DG1 = 20%), the amorphous starch accounted for 60.14%, V-type single helices 6.29%, and the proportion of double helices was 33.56%. In the sample of PT (DG = 20%), the content of amorphous starch was 57.12% and that of double helices was 36.21%, while there were 6.66% V-type single helices. Compared with HT starch, PT starch at a similar DG showed higher single-helix and double-helix relative contents, suggesting that highly-ordered starch structure damaged limitedly under HHP. Additionally, the increase of V-type single helix content in PT starches was believed to be the result of high-pressure making V-type helices more stable compared to those in heat treated granules. In the future study, HHP could as a novel and green method to produce and preserve the V-type crystalline pattern.

3.2. Chain-length distribution of amylopectin

The profiles of amylopectin chain distribution of HT and PT corn starches were examined by HPAEC-PAD (Table 2). The fine structure of amylopectin was divided into four parts according to the degree of polymerization (DP), including A (DP 6–12), B_1 (DP 13–24), B_2 (DP 25–36), and B_3 (DP > 37) chains (Gayin, Abdel-Aal, Manful, & Bertoft, 2016). The A chains as the outmost chains of amylopectin were the shortest and were linked to other chains by their reducing ends through α-1,6 linkages (Jeong, Ju, & Chung, 2021). Furthermore, it has been proposed that shorter amylopectin chains (A and B_1) are responsible for the formation of double helices which involve in crystalline lamellar formation in the starch granules (Bertoft 2017). The B_2, B_3 chains are defined as internal segments and participate in forming the amorphous lamellae. The increasing A chain content occurred in the HT starch with increasing DG, whereas the B_2 and B_3 chains tended to decrease, this phenomenon was probably due to the cleavage of the longer chains by heating. This preferential cleavage suggested that internal B_2 or B_3 chains might be broken at α-1,4 glycosidic linkages in amorphous areas rather than denser crystalline lamellae under heating energy. According to the cluster model proposed by Hizukuri (Hizukuri 1986), B_2 chains penetrate through two clusters and B_3 chains through three clusters, indicating each cluster is part of the repeating crystalline and amorphous lamellae (Lee, Park, Jeong, Chae, & Oh, 2017). Moreover, a deceased proportion of amylopectin internal chains were related to the greater number of crystalline defects appearing in the crystalline lamellae (Witt & Gilbert, 2014). Thus, an increased proportion of A chains ranged from 25.13% to 26.84%, and a decreasing percentage of longer chains, especially B_2 (from 13.01% to 12.09%) and B_3 chains (from 10.64% to 10.09%), contributed to the increase in crystal defects.

Table 1
Structural characteristic of HT and PT corn starch at different DGs determined by ^{13}C CP/MAS NMR and ^{1}H LF-NMR.

Samples	Relative proportion (%)						T_2 (ms)	
	Amorphous phase		Double helix		Single helix			
	HT	PT	HT	PT	HT	PT	HT	PT
DG1 = 20%	$60.14 \pm 0.05^{a***}$	57.12 ± 0.17^{a}	$33.56 \pm 0.13^{a**}$	36.21 ± 0.10^{a}	6.29 ± 0.16^{a}	6.66 ± 0.21^{a}	0.266 ± 0.0^{a}	0.404 ± 0.0^{a}
DG2 = 50%	$67.36 \pm 0.05^{b***}$	65.22 ± 0.17^{b}	$28.62 \pm 0.13^{b**}$	30.09 ± 0.07^{b}	$4.01 \pm 0.17^{b*}$	4.67 ± 0.13^{b}	0.305 ± 0.0^{b}	0.464 ± 0.0^{b}
DG3 = 70%	$75.49 \pm 0.30^{c**}$	73.08 ± 0.05^{c}	$21.22 \pm 0.20^{c**}$	23.16 ± 0.09^{c}	$3.29 \pm 0.18^{c**}$	3.75 ± 0.12^{c}	0.404 ± 0.0^{c}	0.464 ± 0.0^{b}
DG4 = 85%	$80.40 \pm 0.21^{d***}$	77.73 ± 0.30^{d}	$17.05 \pm 0.07^{d**}$	19.32 ± 0.25^{d}	2.54 ± 0.26^{d}	2.94 ± 0.06^{d}	0.464 ± 0.0^{d}	0.464 ± 0.0^{b}
DG5 = 100%	$88.86 \pm 0.17^{e***}$	84.72 ± 0.23^{e}	$10.51 \pm 0.17^{e**}$	13.48 ± 0.26^{e}	$0.63 \pm 0.35^{e*}$	1.79 ± 0.14^{e}	0.464 ± 0.0^{d}	0.534 ± 0.0^{c}

Results are the average of three replicates with standard deviations.
Values in the same column of the same category with the different letters differ significantly ($p < 0.05$).
*Indicates the difference is significant at the 0.05 level, **indicates significance at the 0.01 level, ***indicates significance at the 0.001 level between HT starch and PT starch at a similar DG.

Table 2
Chain length distribution of HT and PT corn starch at different DGs.

Samples	DP (6–12) A (%)		DP (13–24) B_1 (%)		DP (25–36) B_2 (%)		DP (≥37) B_3 (%)	
	HT	PT	HT	PT	HT	PT	HT	PT
Native	24.71 ± 0.04^{f}		50.95 ± 0.06^{f}		13.47 ± 0.05^{f}		10.85 ± 0.08^{f}	
DG = 20%	$25.13 \pm 0.08^{a*}$	24.93 ± 0.05^{a}	51.20 ± 0.19^{a}	51.13 ± 0.04^{a}	$13.01 \pm 0.01^{a*}$	13.25 ± 0.07^{a}	10.64 ± 0.25^{a}	10.68 ± 0.05^{a}
DG = 50%	$25.48 \pm 0.17^{b*}$	25.12 ± 0.05^{b}	51.03 ± 0.03^{b}	51.05 ± 0.04^{ab}	$12.77 \pm 0.05^{b*}$	13.07 ± 0.07^{b}	$10.27 \pm 0.03^{ab*}$	10.76 ± 0.12^{b}
DG = 70%	$25.81 \pm 0.05^{c*}$	25.23 ± 0.07^{b}	51.08 ± 0.03^{b}	51.00 ± 0.05^{b}	$12.53 \pm 0.02^{c*}$	13.04 ± 0.10^{b}	$10.37 \pm 0.14^{b*}$	10.75 ± 0.03^{b}
DG = 85%	$26.24 \pm 0.09^{d***}$	25.45 ± 0.05^{c}	51.07 ± 0.04^{b}	51.01 ± 0.05^{b}	$12.28 \pm 0.05^{d**}$	12.87 ± 0.02^{c}	$10.20 \pm 0.09^{ab*}$	10.65 ± 0.07^{b}
DG = 100%	$26.84 \pm 0.06^{e**}$	25.85 ± 0.08^{d}	50.97 ± 0.06^{c}	50.93 ± 0.04^{c}	$12.09 \pm 0.06^{e***}$	12.77 ± 0.07^{c}	$10.09 \pm 0.06^{c*}$	10.44 ± 0.09^{b}

Results are the average of three replicates with standard deviations.
Values in the same column of the same category with the different letters differ significantly ($p < 0.05$).
*Indicates the difference is significant at the 0.05 level, **indicates significance at the 0.01 level, ***indicates significance at the 0.001 level between HT starch and PT starch at a similar DG.

These results could explain the decrease in double and single helices after heating gelatinization as verified by the ^{13}C CP/MAS NMR results. This result was also in agreement with the changes in relative crystallinity and d_a values determined by XRD and SAXS in our previous research (Liu et al., 2020). PT starches have chains that are on average longer than those of HT starches at similar DG and have more B_2 and B_3 chains retained with restricted degradation. This result may be because pressure hinders the degradation of longer external segments compared to heating at a similar DG. HHP might promote the stability of the branching point of amylopectin which has been proposed to protect the integrity of crystal form in PT starches. Longer amylopectin chains could possibly promote more ordered packing of double helices and crystals inside starch granules (Vamadevan & Bertoft, 2018). We hypothesize that heating gelatinization might cause more breakage of α-1,4-glycosidic bonds than does high pressure.

3.3. Molecular weight measurement

The molecular weight distribution of HT and PT corn starch showed a typical bimodal distribution pattern (Fig. 2). Amylopectin (M_w was about 1×10^7-5×10^8 g/mol) were eluted earlier, while the smaller components (M_w was about 1×10^5-1×10^6 g/mol) in the samples are eluted later (Bxa et al., 2020). As the DG increased, the second peak in the refractive index for HT and PT starch became broader and higher. This result means that the corn starch is degraded into smaller fractions after heating and pressurizing. As seen in Table 3, the weight-average molecular mass (M_w) of native corn starch was 1.03×10^8 g/mol. A significant decrease in the M_w value in the HT starches compared with the PT starches was exhibited. Heating significantly reduced molecular weights even one third of the native corn starch at 100% DG for 3.25×10^7 g/mol. The M_w decrease in modified corn starch could be attributed to the depolymerization of starch molecules by breaking hydrogen bonds. Similar results were also found by (Yu et al., 2020). In terms of the molecular structure of HT starches, heating resulted in greater amylopectin breakage and degradation, and the destruction of ordered

Table 3
Molecular parameters of HT and PT corn starch at different DGs.

Samples	$M_w \times 10^7$ (g/mol)		Polydispersity (M_w/M_n)		R_z (nm)	
	HT	PT	HT	PT	HT	PT
Native	10.30 ± 0.21^{a}		3.43 ± 0.02^{a}		234.2 ± 1.34^{a}	
DG = 20%	$6.23 \pm 0.11^{b*}$	6.25 ± 0.09^{a}	$3.88 \pm 0.03^{b**}$	3.78 ± 0.03^{b}	$193.1 \pm 1.42^{b*}$	197.7 ± 1.14^{b}
DG = 50%	$5.16 \pm 0.13^{c***}$	6.56 ± 0.19^{b}	$3.420 \pm 0.02^{c*}$	3.50 ± 0.02^{c}	$172 \pm 1.23^{c***}$	195.1 ± 1.24^{c}
DG = 70%	$5.08 \pm 0.15^{d**}$	5.42 ± 0.11^{c}	$3.13 \pm 0.05^{d***}$	3.82 ± 0.04^{d}	$168.2 \pm 0.84^{d***}$	186.6 ± 1.76^{d}
DG = 85%	$4.32 \pm 0.14^{e***}$	5.37 ± 0.12^{d}	$3.35 \pm 0.03^{e**}$	3.52 ± 0.05^{e}	$154.8 \pm 0.85^{e***}$	180.5 ± 0.35^{e}
DG = 100%	$3.25 \pm 0.12^{f***}$	4.05 ± 0.12^{e}	$2.30 \pm 0.01^{f***}$	2.81 ± 0.06^{f}	$145.7 \pm 0.65^{f***}$	165.8 ± 1.09^{f}

Results are the average of three replicates with standard deviations.
Values in the same column of the same category with the different letters differ significantly ($p < 0.05$).
*Indicates the difference is significant at the 0.05 level, **indicates significance at the 0.01 level, ***indicates significance at the 0.001 level between HT starch and PT starch at a similar DG.

structure was more significant and drastic. Specifically, the M_w value of PT2 granules tended to be the highest for 6.56×10^7 g/mol ($p < 0.05$), which was probably due to the entanglement between amylose and longer amylopectin under lower pressure treatment. Hence, we postulate that pressure gelatinization is not a simple and single-direction process which is unlike heat gelatinization.

Polydispersity (PDI = M_w/M_n) is a criterion for reflecting the uniformity dispersity of polymers based on the size (Hoyos-Leyva, Bello-Pérez, Alvarez-Ramirez, & Agama-Acevedo, 2017). The differences in

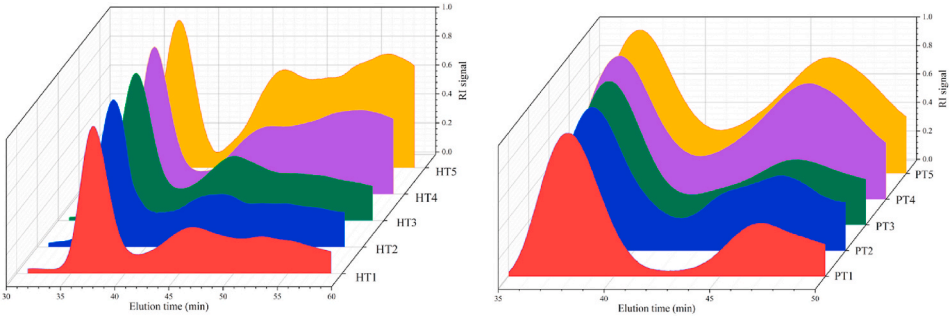

Fig. 2. The molecular weight distribution and parameters of HT and PT corn starch at various approximate DGs determined by HPSEC-MALLS-RI (HT1 and PT1,20% DG; HT2 and PT2, 50% DG; HT3 and PT3, 70% DG; HT4 and PT4,85% DG; HT5 and PT5, 100% DG).

the molecular mass distributions of HT and PT corn starch can be conducted by comparing the molar mass dispersity. The PDI of HT and PT starches (DG from 20% to 100%) decreased from 3.88 to 2.30 and from 3.78 to 2.81, respectively (Table 2). This phenomenon indicates that degradation after heating results in a more homogeneous molecular weight distribution. Similarly, the M_w/M_n ratio decreased from 3.43 for native corn starch to 2.30 for starch pressurized at 600 MPa in previous research (Szwengiel, Lewandowicz, Górecki, & Błaszczak, 2018).

The Z-average radius of gyration (R_z) can be affected by the structure as well as the length of branched amylopectin chains (Wei, Cai, Xu, Jin, & Tian, 2018). The reduction of R_z in HT and PT starches reflected the decrease in the extent of branching, indicating that heat and pressure modification damaged not only α-1,4 glycosidic linkages but also α-1,6 glycosidic linkages of starch. The R_z value in PT starch was higher than that of HT starch at similar DG, which may be related to a greater loss of branching in HT starch. The presence of amylopectin with a larger ratio of long branched chains in PT starch might increase R_z. The M_w and R_z changes are in good agreement with the results from HPAEC-PAD analysis.

3.4. ^1H NMR spectroscopy

^1H NMR analysis was conducted to determine the molecular structure of HT and PT corn starch, and the spectra was presented in Fig. 3. Due to the high sensitivity of ^1H NMR, the resolution of the anomeric proton resonances of starch was detected when the chemical environment of hydrogen is changed (Liu, Adhikari, Guo, & Adhikari, 2013). The residual DMSO signal (2.49 nm) was used to calculate the chemical shift scale. Typically, the α-1,4-glycosidic bonds corresponded to 5.11 ppm and the chemical shift of α-1,6-glycosidic bonds was 4.75 ppm (Tizzotti, Sweedman, Tang, Schaefer, & Gilbert, 2011). Starch is a simple molecule which have many glucose units linked by α-(1, 4) linkages with branching by α-(1, 6) linkages (Pérez & Bertoft, 2010). Compared to the spectrum of native corn starch, the anomeric signals of α-1,4-linkages in HT and PT starches were weaker to various degrees, showing that heat and pressure modification changed proton chemical environments. Furthermore, the relative intensity of peaks (α-1, 4-glycosidic bonds) in HT starches were lower than in PT starches, indicating that heating could partially crack the amylose and amylopectin into shorter chains through the α-1,4-glycosidic bonds. This conclusion was consistent with chain length distribution results (Szwengiel et al., 2018). found that in pressurized waxy maize starch, the α-1,6 bonds are most often split compared with α-1,4 bonds. This may be attributed to that HHP resulted in strong interactions between amylose and amylopectin which contributed to a compact structure. In this study, the signals of α-1,6 glycosidic bonds were not detected in HT and PT corn starches, which might be due to higher sensitives than α-1,4 bonds under heating and HHP.

3.5. Water distribution (LF-NMR spectroscopy)

LF-NMR spectroscopy is used as an effective and convenient technique to investigate the distribution and migration of water in food matrices (Chen et al., 2019). Measurements are focused on the transverse relaxation spectra (T_2) of the HT and PT corn starch, obtained from CPMG tests (Fig. 4). T_2 is the time required for an excited spin-spin proton to reach dynamic equilibrium after energy exchange with the surrounding protons, which excludes effects of the heterogeneous magnetic field (Pitombo & Lima, 2003). In starch granules, T_2 is dominated by fast exchange of protons between water and starch hydroxyl groups. The right shift of T_2 suggested that the water molecules had higher degrees of freedom, i.e., the water and starch molecules were weakly combined (Fig. 4). There was a general increase in T_2 for HT and PT starches with increasing DG (Table 1), meaning that high temperature and pressure constantly disrupted the internal network structure of the starch molecules and that the immobilized water molecules might become more flexible. This indicated that fragmentation and melting of the ordered structure facilitating the interaction between starch and water molecules. In the HT (DG2 = 50%, DG3 = 70%, DG4 = 85%) samples, T_2 values presented a dynamically upward trend (from 0.305 to 0.464 ms) with increasing DG, indicating that starch molecules would dissociate and disaggregate step by step during heating gelatinization. However, T_2 values stayed constant and were always 0.464 ms for PT ((DG2 = 50%, DG3 = 70%, DG4 = 85%). Only one single peak for bound water could be detected for A-type starch due to the small size of A-type starch, as described by (Tang, Godward, & Hills, 2000). Compared with HT starch, PT starch at similar DG exhibited a higher value of T_2, which suggested that HHP reduced the binding of immobilized water and raised freedom degree of water. According to the previous study (Luo, He, Fu, Luo, & Gao, 2006), A-type starch might transform into B-type where double helices were packed with 36 inter-helical water molecules at a pressure of 600 MPa, generating a hydrated central cavity. However, in A-type starch crystallites, double helices are tightly packed with only four inter-helical water molecules and the center of the lattice contains a pair of double helices (Pérez & Bertoft, 2010). The stronger HHP energy would be expected to make more regions available for binding with water molecules, whereas binding capacity of PT starch was weaker than that of HT starch, which may result from its looser double helices packing mode.

4. Molecular dynamics simulation

4.1. Hydrogen bonds

MD is a useful computer simulation method for studying hydrogen bonding interaction in macromolecules (Yu et al., 2020). Since starch gelatinization depend on the existence of hydrogen-bonding solvent such as water molecules, which has a high number of hydroxyl groups to

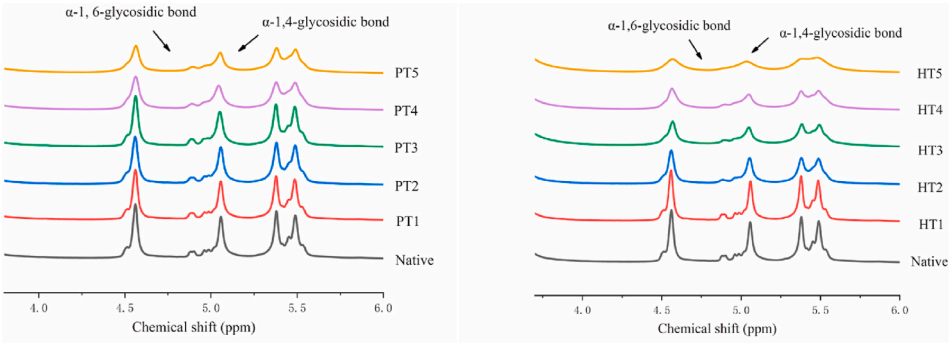

Fig. 3. ^1H NMR spectra of HT and PT corn starch at various approximate DGs (HT1 and PT1, 20% DG; HT2 and PT2,50% DG; HT3 and PT3 70% DG; HT4 and PT4 85% DG; HT5 and PT5,100% DG).

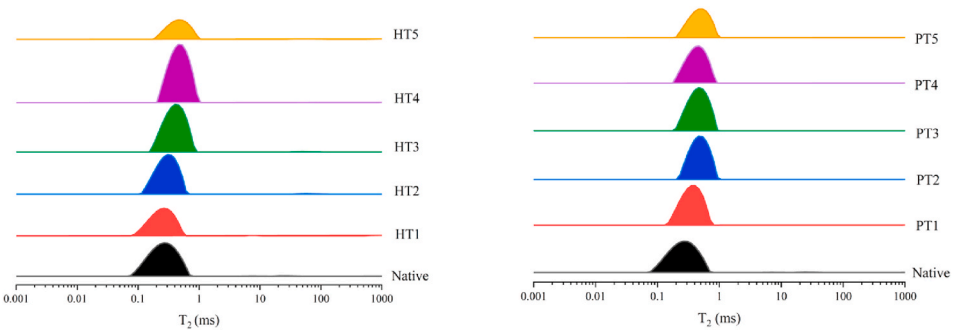

Fig. 4. The LF-NMR transverse relaxation spectrum of HT and PT corn starch at various approximate DGs (HT1 and PT1, 20% DG; HT2 and PT2,50% DG; HT3 and PT3 70% DG; HT4 and PT4 85% DG; HT5 and PT5,100% DG).

form hydrogen bonds (Özeren, Olsson, Nilsson, & Hedenqvist, 2020). Hydrogen bonding plays a critical role in the structural and physicochemical properties of starch. The effect of heating and HHP treatment on the inter- and intra-molecular hydrogen bonds of left-hand helix and V-type amylose are presented in Table 4 and Table 5. In HT and PT amylose, the ordered helix transitioned to a disordered coil during the gelatinization process, and the typical conformations of amylose molecules using MD simulation under different temperature and pressure were shown in Supplementary Fig. 2.

In amylose-water systems, the carbon atoms on single glucose units are generally labeled as C_1, C_2, C_3, C_4, C_5, C_6 respectively, whereas the corresponding oxygen atom connected with the relative carbon atoms is labeled O_1, O_2, O_3, O_5, O_6 (Błaszczak et al., 2011; Cui et al., 2020). The O_2–O_3 and O_6–O_6 intramolecular hydrogen bonds in neighboring glucose units was formed, and their detected number in both HT and PT left-hand and V-type helix exhibited a declined trend with increasing temperature and pressure levels (Table 4). However, the extent of decrease was not significant indicating that O_2–O_3 and O_6–O_6 intramolecular hydrogen bonds were less affected by different temperature and pressure. The starch-water gel modified by heating and HHP treatment was not only through hydrogen bonds along adjacent chains but also Van der Waals forces (VDW). Thus, the unwinding of amylose helical structure might be mainly due to the VDW changes. Besides that, it can be speculated that the inter-molecular hydrogen bonding interaction have a bigger impact on the integrity of amylose.

In terms of intermolecular hydrogen bonds, the total amylose-water hydrogen bonds (both as acceptors and donors) of both HT and PT amylose were predicted to amplify gradually when heating from 65 to 75 °C and pressurizing from 400 to 600 MPa (Table 5). Furthermore, it was obvious that PT amylose built more amylose-water hydrogen bonding than did HT amylose. This difference appeared to be caused by hydrating the amorphous region more serious owning to that pressure was beneficial to force the water into the phase comprised of amylose molecules. In addition, HHP more than heating tended to make water serve as a plasticizer of the amorphous region. These results agreed with the T_2 values acquired by ^{1}H LF-NMR. On the other hand, the intermolecular hydrogen bonds between the starch chains and the water molecules restrict the movement of the molecular chains, hence, which could explain the stabilization and less degradation of the starch chains under HHP conditions.

Table 4
The numbers intramolecular hydrogen bond of HT and PT left-hand and V-type helices modified under different temperature and pressure.

Left-hand helix	O_2–O_3	O_6–O_6	V-type	O_2–O_3	O_6–O_6
65 °C	107.67 ± 0.56^{a}	140.33 ± 0.49^{a}	65 °C	107.67 ± 0.47^{a}	144.0 ± 0.23^{a}
70 °C	103.67 ± 0.32^{b}	132.67 ± 0.23^{b}	70 °C	103.33 ± 0.56^{b}	132.67 ± 0.51^{b}
75 °C	101.67 ± 0.45^{c}	130.67 ± 0.75^{c}	75 °C	101.67 ± 0.29^{c}	131.33 ± 0.74^{c}
400 MPa	111.33 ± 0.76^{ab}	142.33 ± 0.34^{ab}	400 MPa	111.33 ± 0.78^{ab}	142.67 ± 0.89^{ab}
500 MPa	108.67 ± 0.43^{bc}	136.67 ± 0.29^{bc}	500 MPa	108.67 ± 0.67^{bc}	135.67 ± 0.34^{b}
600 MPa	105.33 ± 0.63^{cd}	133.67 ± 0.33^{cd}	600 MPa	105.33 ± 0.45^{cd}	136.0 ± 0.61^{cd}

Results are the average of three replicates with standard deviations.
Values in the same column of the same category with the different letters differ significantly ($p < 0.05$).

4.2. Energies

The stability of starch molecules can be determined by bond stretching, angle bending, dihedral angle torsion, VDW, and electrostatic energies (Zhi-guang et al., 2020). It is believed that the lower the total energies are, the more stable the model will be. In the present study, to verify the mechanisms of heating and HHP gelatinization, three temperatures (65, 70, 75 °C) and three pressures (400, 500, 600 MPa) were applied in the simulation. In both the PT left-hand and V-type helices, the bond stretching vibration and angle bending energies, which were classified into bonding-related energies, reduced slightly from 400 to 600 MPa (Table 5), suggesting that HHP stabilizes the bonds of the starch molecule. In contrast, an obvious rise is seen with increasing temperature. Compared to PT starches, the HT starches had higher bond stretching vibration, angle bending, and dihedral angle torsion amplitude energies, but lower VDW and electrostatic forces. This result could explain why heating had a greater impact on degradation of starches, and caused a preferential breakage α-1,4-glycosidic bonds and α-1, 6-glycosidic bonds. Additionally, the stabilization of double-helices formed by sidechains of amylopectin or amylose was maintained via not only hydrogen-bonding interaction but also by VDW and electrostatic forces. Furthermore, 60% of the stabilization was from VDW forces (Imberty, Chanzy, Pérez, Bulèon, & Tran, 1988). The higher VDW in PT starches resulted from amylose helix unwinding facilitated by HHP. This unwinding could also explain why PT starches exhibited more amylose-water hydrogen bonds instead of intramolecular hydrogen bonds between starch molecules. Thus, the mechanisms of gelatinization differed between HT and PT processing. These results are consistent with previous research, namely that the gelatinization mechanisms of heating and HHP differ (Chen et al., 2019). The schematic diagrams (Fig. 5) reveal various molecular mechanisms of HT and PT gelatinization which may assist food industry scientists in designing starch granules with specific structures.

5. Conclusions

In the present study, the combination of ^{13}C CP/MAS NMR, HPAEC-PAD, GPC-MALLS-RI, ^{1}H NMR and LF-NMR used here could estimate that the molecular structure of HT and PT corn starches varied at similar

Table 5
The numbers of amylose-water hydrogen bond and energies of HT and PT left-hand and V-type helices modified under different temperature and pressure.

Left-hand helix	Acceptor O_2	Acceptor O_3	Acceptor O_6	Acceptor O_5	Donor O_2	Donor O_3	Donor O_6	Bond stretching vibration	Angle bending	Dihedral angle torsion amplitude	Electrostatic energy	VDW
HT												
65 °C	121.33 ± 0.54^{a}	134.33 ± 1.05^{c}	166.67 ± 0.56^{a}	41.67 ± 0.37^{a}	95.67 ± 1.21^{a}	94.67 ± 0.24^{a}	173.33 ± 0.67^{a}	632.14 ± 1.60^{a}	1394.42 ± 1.21^{a}	3253.99 ± 2.72^{a}	−8435.94 ± 2.81^{a}	−320.678 ± 1.13^{a}
70 °C	121.33 ± 0.94^{a}	138.33 ± 0.63^{b}	169.33 ± 0.24^{b}	42.67 ± 0.45^{b}	99.33 ± 1.07^{b}	98.33 ± 0.45^{b}	174.67 ± 0.76^{b}	637.58 ± 1.73^{b}	1410.99 ± 4.26^{b}	3257.37 ± 2.31^{b}	−8429.18 ± 4.59^{a}	−315.737 ± 1.05^{b}
75 °C	125.67 ± 1.08^{b}	139.67 ± 0.78^{a}	172.33 ± 0.71^{c}	44.33 ± 0.75^{c}	100.67 ± 1.54^{c}	102.33 ± 0.35^{c}	176.33 ± 0.66^{c}	643.92 ± 0.44^{c}	1431.28 ± 0.56^{c}	3259.20 ± 1.27^{c}	−8431.12 ± 5.81^{a}	−308.595 ± 1.11^{c}
PT												
400 MPa	137.67 ± 1.68^{a}	160.67 ± 1.34^{a}	180.0 ± 0.24^{a}	45.67 ± 1.00^{a}	114.67 ± 0.46^{a}	120.0 ± 1.03^{a}	187.33 ± 0.63^{a}	587.53 ± 1.92^{a}	1289.46 ± 5.90^{a}	3221.86 ± 3.27^{a}	−8428.95 ± 0.64^{a}	−303.83 ± 1.67^{a}
500 MPa	139.0 ± 0.67^{a}	160.67 ± 0.90^{a}	186.67 ± 0.34^{b}	46.67 ± 1.05^{a}	116.67 ± 0.77^{b}	123.33 ± 0.87^{a}	188.33 ± 0.45^{a}	584.42 ± 0.59^{b}	1284.30 ± 5.88^{a}	3223.51 ± 3.83^{a}	−8424.96 ± 1.11^{b}	−296.98 ± 0.65^{b}
600 MPa	147.33 ± 1.24^{b}	162.67 ± 0.35^{b}	190.33 ± 0.22^{c}	50.33 ± 0.82^{b}	117.0 ± 0.35^{b}	126.0 ± 0.43^{b}	191.67 ± 1.33^{a}	582.83 ± 1.40^{b}	1282.93 ± 3.34^{a}	3224.63 ± 2.86^{a}	−8416.88 ± 1.22^{c}	−295.14 ± 1.96^{b}
V-type HT												
65 °C	83.67 ± 0.56^{a}	84.67 ± 0.46^{a}	103.67 ± 0.92^{a}	67.67 ± 0.95^{a}	155.67 ± 0.74^{a}	112.67 ± 0.43^{a}	165.0 ± 0.67^{a}	644.45 ± 0.86^{a}	1484.89 ± 4.70^{a}	3068.21 ± 1.21^{a}	−8624.72 ± 9.90^{a}	−344.68 ± 7.02^{a}
70 °C	87.0 ± 1.95^{b}	86.67 ± 0.28^{b}	105.67 ± 0.45^{a}	69.0 ± 0.57^{a}	160.0 ± 0.89^{b}	117.67 ± 0.83^{b}	168.33 ± 0.83^{b}	654.83 ± 2.16^{b}	1502.80 ± 8.15^{b}	3072.66 ± 1.81^{a}	−8597.89 ± 8.21^{ab}	−326.19 ± 1.49^{ab}
75 °C	89.67 ± 1.90^{b}	87.33 ± 0.31^{b}	111.67 ± 0.32^{b}	72.0 ± 0.29^{b}	162.0 ± 0.22^{c}	123.67 ± 0.35^{c}	169.67 ± 0.73^{b}	661.55 ± 3.15^{c}	1520.68 ± 5.66^{c}	3085.77 ± 4.01^{b}	−8585.21 ± 5.71^{b}	−314.00 ± 6.13^{b}
PT												
400 MPa	100.0 ± 1.38^{a}	89.0 ± 0.13^{a}	120.33 ± 0.22^{a}	71.33 ± 0.45^{a}	173.0 ± 0.64^{a}	124.33 ± 0.64^{a}	179.67 ± 0.88^{a}	599.18 ± 2.02^{ab}	1375.80 ± 2.26^{a}	3050.85 ± 9.94^{a}	−8605.23 ± 1.04^{a}	−320.384 ± 1.67^{a}
500 MPa	103.67 ± 1.77^{b}	91.67 ± 0.33^{b}	124.67 ± 0.78^{b}	75.33 ± 0.81^{b}	182.33 ± 0.35^{a}	136.67 ± 0.46^{b}	181.67 ± 0.82^{a}	600.07 ± 1.23^{b}	1372.09 ± 6.32^{ab}	3043.34 ± 9.78^{a}	−8595.08 ± 0.67^{b}	−310.932 ± 2.01^{b}
600 MPa	107.67 ± 1.40^{c}	94.67 ± 1.03^{c}	128.67 ± 1.52^{c}	77.33 ± 0.78^{c}	183.33 ± 0.34^{a}	139.33 ± 0.59^{c}	183.33 ± 0.38^{b}	594.61 ± 3.13^{a}	1365.02 ± 3.13^{b}	3055.36 ± 5.06^{a}	−8579.62 ± 1.01^{c}	−305.286 ± 1.07^{c}

Results are the average of three replicates with standard deviations.
Values in the same column of the same category with the different letters differ significantly ($p < 0.05$).

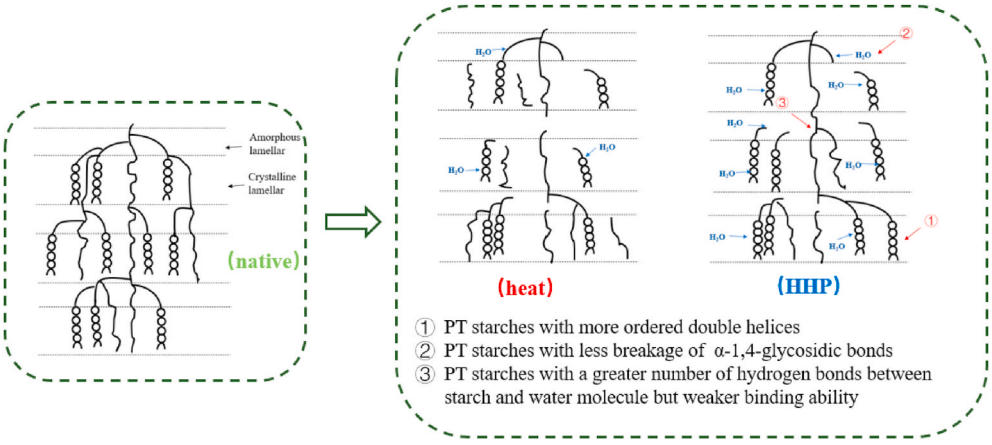

Fig. 5. Schematic diagrams of starch-water interaction under the HT and PT starch gelatinization.

DGs. Compared with PT starches, a higher proportion of A chains but a larger drop in longer B_2 and B_3 chains were observed due to drastic degradation by heating. Moreover, the α-1,4-glycosidic bonds were broken more frequently with lower molecular weight in HT starches.

Our results also indicate that HHP reduces the binding of immobilized water and raises freedom degree of water molecules. MD simulation was employed to provide supporting evidence on the intra- and inter-hydrogen bonding interactions in HT and PT amylose-water systems. HHP tends to make water serve as a plasticizer of the amorphous region more than heating. The differences regarding to energy change during heating and HHP gelatinization which can be summarized as follows: higher bonding-related energies, but lower VDW interactions occurred in heating gelatinization than in HHP gelatinization, which agreed well with the experimental data.

In summary, the experimental data combined with MD simulation have the potential to be valuable methods to investigate the various mechanisms of heating and HHP gelatinization. HHP gelatinization is not a constant process like heating one with a single trend and there may be a critical point or threshold from “zero” to “perfect” gelatinization during HHP gelatinization. This research probably opens a new avenue to design given starch-based products in an environmental-friendly and energy-efficient way.

CRediT authorship contribution statement

Zhenyu Liu: Methodology, Formal analysis, Writing – original draft,

Writing – review & editing. **Yongxia Fu:** Validation. **Fan Zhang:** Visualization. **Qingyu Zhao:** Data curation. **Yong Xue:** Supervision. **Jinrong Hu:** Conceptualization. **Qun Shen:** Project administration.

Declaration of competing interest

The authors declare that they have no known competing financial interests or personal relationships that could have appeared to influence the work reported in this paper.

Acknowledgements

We would like to thank the financial support from the National Natural Science Foundation of China (code: 32072136). Dr. Zhenyu Liu are grateful to Dr. Zerui Li for his technical guidance in this paper.

Appendix A. Supplementary data

Supplementary data to this article can be found online at https://doi.org/10.1016/j.foodhyd.2021.107371.

References

Al-Ansi, W., Sajid, B. M., Mahdi, A. A., Al-Maqtari, Q. A., Al-Adeeb, A., Ahmed, A., Fan, M., Li, Y., Qian, H., Jinxin, L., & Wang, L. (2021). Molecular structure, morphological, and physicochemical properties of highlands barley starch as affected by natural fermentation. *Food Chemistry, 356*, 129665.

BeMiller, J. N., & Huber, K. C. (2015). Physical modification of food starch functionalities. *Annual Review of Food Science and Technology, 6*(1), 19–69.

Berendsen, H. J. C., der Spoel, D.van, & van, R. (1995). Gromacs: A message-passing parallel molecular dynamics implementation - ScienceDirect. *Computer Physics Communications, 91*(1–3), 43–56.

Bertoft, E. (2017). Understanding starch structure: Recent progress. *Agronomy, 7*(3), 56.

Błaszczak, W., Bidzińska, E., Dyrek, K., Fornal, J., Michalec, M., & Wenda, E. (2011). Effect of phosphorylation and pretreatment with high hydrostatic pressure on radical processes in maize starches with different amylose contents. *Carbohydrate Polymers, 85*(1), 86–96.

Bxa, D., Ar, B., Jc, A., Hl, C., Bw, A., Jing, W. C., Smraa, D., Bb, E., Cza, D., & Hma, D. (2020). Effect of multi-mode dual-frequency ultrasound irradiation on the degradation of waxy corn starch in a gelatinized state - ScienceDirect. *Food Hydrocolloids*.

Chen, C., Fu, W., Chang, Q., Zheng, B., Zhang, Y., & Zeng, H. (2019). Moisture distribution model describes the effect of water content on the structural properties of lotus seed resistant starch. *Food Chemistry, 286*, 449–458.

Cheng, L., Feng, T., Zhang, B., Zhu, X., Hamaker, B., Zhang, H., & Campanella, O. (2018). A molecular dynamics simulation study on the conformational stability of amylose-linoleic acid complex in water. *Carbohydrate Polymers, 196*, 56–65.

Chen, Z. G., Huang, J. R., Pu, H. Y., Yang, Q., & Fang, C. L. (2020). The effects of HHP (high hydrostatic pressure) on the interchain interaction and the conformation of amylopectin and double-amylose molecules. *International Journal of Biological Macromolecules, 155*.

Cui, F., Zi, H., Liu, H., Zhang, S., & Yuan, B. (2020). A study of starch-urea-water mixtures with a combination of molecular dynamics simulation and traditional characterization methods. *International Journal of Biological Macromolecules, 148*, 121–128.

Fan, D., Ma, S., Wang, L., Zhao, H., Zhao, J., Zhang, H., & Chen, W. (2013). 1H NMR studies of starch–water interactions during microwave heating. *Carbohydrate Polymers, 97*(2), 406–412.

Feng, T., Li, M., Zhou, J., Zhuang, H., Chen, F., Ye, R., Campanella, O., & Fang, Z. (2015). Application of molecular dynamics simulation in food carbohydrate research—a review. *Innovative Food Science & Emerging Technologies, 31*, 1–13.

Gayin, J., Abdel-Aal, E.-S. M., Manful, J., & Bertoft, E. (2016). Unit and internal chain profile of African rice (Oryza glaberrima) amylopectin. *Carbohydrate Polymers, 137*, 466–472.

Hizukuri, S. (1986). Polymodal distribution of the chain lengths of amylopectins, and its significance. *Carbohydrate Research, 147*(2), 342–347.

Hoyos-Leyva, J. D., Bello-Pérez, L. A., Alvarez-Ramirez, J., & Agama-Acevedo, E. (2017). Structural characterization of aroid starches by means of chromatographic techniques. *Food Hydrocolloids, 69*, 97–102.

Imberty, A., Chanzy, H., Pérez, S., Buléon, A., & Tran, V. (1988). The double-helical nature of the crystalline part of A-starch. *Journal of Molecular Biology, 201*(2), 365–378.

Jacobs, H., & Delcour, J. A. (1998). Hydrothermal modifications of granular starch, with retention of the granular structure: A review. *Journal of Agricultural and Food Chemistry, 46*(8), 2895–2905.

Jeong, D., Ju, H. L., & Chung, H. J. (2021). Effect of molecular structure on phase transition behavior of rice starch with different amylose contents. *Carbohydrate Polymers*, 117712.

Larrea-Wachtendorff, D., Di Nobile, G., & Ferrari, G. (2020). Effects of processing conditions and glycerol concentration on rheological and texture properties of starch-based hydrogels produced by high pressure processing (HPP). *International Journal of Biological Macromolecules, 159*, 590–597.

Lee, S. J., Park, S.-H., Jeong, A., Chae, H., & Oh, K. (2017). Temperamental predictors of developmental trajectories of inattention and hyperactivity–impulsivity problems in schoolchildren. *Integrative Medicine Research, 6*(1), 33–40.

Li, C., & Gong, B. (2020). Insights into chain-length distributions of amylopectin and amylose molecules on the gelatinization property of rice starches. *International Journal of Biological Macromolecules, 155*, 721–729.

Li, C., Oh, S.-G., Lee, D.-H., Baik, H.-W., & Chung, H.-J. (2017). Effect of germination on the structures and physicochemical properties of starches from brown rice, oat, sorghum, and millet. *International Journal of Biological Macromolecules, 105*, 931–939.

Liu, H., Adhikari, R., Guo, Q., & Adhikari, B. (2013). Preparation and characterization of glycerol plasticized (high-amylose) starch–chitosan films. *Journal of Food Engineering, 116*(2), 588–597.

Liu, Z., Wang, C., Liao, X., & Shen, Q. (2020). Measurement and comparison of multi-scale structure in heat and pressure treated corn starch granule under the same degree of gelatinization. *Food Hydrocolloids, 108*, 106081.

Li, G., Zhu, F., Mo, G., & Hemar, Y. (2019). Supramolecular structure of high hydrostatic pressure treated quinoa and maize starches. *Food Hydrocolloids, 92*, 276–284.

Luo, Z., He, X., Fu, X., Luo, F., & Gao, Q. (2006). Effect of microwave radiation on the physicochemical properties of normal maize, waxy maize and amylomaize V starches. *Starch - Stärke, 58*(9), 468–474.

Lu, J., Qiu, Y., Baron, R., & Molinero, V. (2014). Coarse-graining of TIP4P/2005, TIP4P-ew, SPC/E, and TIP3P to monatomic anisotropic water models using relative entropy minimization. *Journal of Chemical Theory and Computation, 10*(9), 4104–4120.

Mja, A., Tm, D., Rsb, C., Sp, A., Jcsb, C., Bh, A., & Ela, D. (2015). Gromacs: High performance molecular simulations through multi-level parallelism from laptops to supercomputers - ScienceDirect. *SoftwareX s, 1–2*, 19–25.

Monroy, Y., Rivero, S., & García, M. A. (2018). Microstructural and techno-functional properties of cassava starch modified by ultrasound. *Ultrasonics Sonochemistry, 42*, 795–804.

Özeren, H. D., Olsson, R. T., Nilsson, F., & Hedenqvist, M. S. (2020). Prediction of plasticization in a real biopolymer system (starch) using molecular dynamics simulations. *Materials & Design, 187*, 108387.

Paris, M., Bizot, H., Emery, J., Buzaré, J. Y., & Buléon, A. (1999). Crystallinity and structuring role of water in native and recrystallized starches by 13C CP-MAS NMR spectroscopy: 1: Spectral decomposition. *Carbohydrate Polymers, 39*(4), 327–339.

Pei-Ling, L., Xiao-Song, H., & Qun, S. (2010). Effect of high hydrostatic pressure on starches: A review. *Starch - Stärke, 62*(12), 615–628.

Pérez, S., & Bertoft, E. (2010). The molecular structures of starch components and their contribution to the architecture of starch granules: A comprehensive review. *Starch - Stärke, 62*(8), 389–420.

Pitombo, R. N. M., & Lima, G. A. M. R. (2003). Nuclear magnetic resonance and water activity in measuring the water mobility in Pintado (Pseudoplatystoma corruscans) fish. *Journal of Food Engineering, 58*(1), 59–66.

Price, D. J., & Brooks, C. L. (2004). A modified TIP3P water potential for simulation with Ewald summation. *The Journal of Chemical Physics, 121*(20), 10096–10103.

Rca, B., Js, A., Lk, A., Edrz, B., Argd, B., Rbs, C., & Hs, A. (2017). Microstructural characteristics and gastro-small intestinal digestion in vitro of potato starch: Effects of refrigerated storage and reheating in microwave. *Food Chemistry, 226*, 171–178.

Sandhu, K. S., Kaur, M., Punia, S., & Ahmed, J. (2021). Rheological, thermal, and structural properties of high-pressure treated Litchi (Litchi chinensis) kernel starch. *International Journal of Biological Macromolecules, 175*, 229–234.

Schafranski, K., Ito, V. C., & Lacerda, L. G. (2021). Impacts and potential applications: A review of the modification of starches by heat-moisture treatment (HMT). *Food Hydrocolloids, 117*, 106690.

Šoltýs, A., Hronský, V., Šmídová, N., Olčák, D., Ivanič, F., & Chodák, I. (2019). Solid-state 1H and 13C NMR of corn starch plasticized with glycerol and urea. *European Polymer Journal, 117*, 19–27.

Spoel, D., Lindahl, E., Hess, B., Groenhof, G., & Berendsen, H. (2005). Gromacs: Fast, flexible, and free. *Journal of Computational Chemistry, 26*(16), 1701–1718.

Szwengiel, A., Lewandowicz, G., Górecki, A. R., & Błaszczak, W. (2018). The effect of high hydrostatic pressure treatment on the molecular structure of starches with different amylose content. *Food Chemistry, 240*, 51–58.

Takeda, Y., Takeda, C., Mizukami, H., & Hanashiro, I. (1999). Structures of large, medium and small starch granules of barley grain. *Carbohydrate Polymers, 38*(2), 109–114.

Tan, I., Flanagan, B. M., Halley, P. J., Whittaker, A. K., & Gidley, M. J. (2007). A method for estimating the nature and relative proportions of amorphous, single, and double-helical components in starch granules by 13C CP/MAS NMR. *Biomacromolecules, 8*(3), 885–891.

Tang, H. R., Godward, J., & Hills, B. (2000). The distribution of water in native starch granules—a multinuclear NMR study. *Carbohydrate Polymers, 43*(4), 375–387.

Tizzotti, M. J., Sweedman, M. C., Tang, D., Schaefer, C., & Gilbert, R. G. (2011). New 1H NMR procedure for the characterization of native and modified food-grade starches. *Journal of Agricultural and Food Chemistry, 59*(13), 6913–6919.

Vamadevan, V., & Bertoft, E. (2018). Impact of different structural types of amylopectin on retrogradation. *Food Hydrocolloids, 80*, 88–96.

Wei, B., Cai, C., Xu, B., Jin, Z., & Tian, Y. (2018). Disruption and molecule degradation of waxy maize starch granules during high pressure homogenization process. *Food Chemistry, 240*, 165–173.

Witt, T., & Gilbert, R. G. (2014). Causal relations between structural features of amylopectin, a semicrystalline hyperbranched polymer. *Biomacromolecules, 15*(7), 2501–2511.

Yu, W.-W., Zhai, H.-L., Xia, G.-B., Tao, K.-Y., Li, C., Yang, X.-Q., & Li, L.-H. (2020). Starch fine molecular structures as a significant controller of the malting, mashing, and fermentation performance during beer production. *Trends in Food Science & Technology, 105*, 296–307.

Zhi-guang, C., Hong-hui, Z., Keipper, W., Hua-yin, P., Qi, Y., Chen-lu, F., Guo-wei, S., & Jun-rong, H. (2020). The analysis of the effects of high hydrostatic pressure (HHP) on amylose molecular conformation at atomic level based on molecular dynamics simulation. *Food Chemistry, 327*, 127047.

Zhong, Z., & Sun, X. S. (2005). Thermal characterization and phase behavior of cornstarch studied by differential scanning calorimetry. *Journal of Food Engineering, 69*(4), 453–459.

Zhu, F. (2017). Structures, physicochemical properties, and applications of amaranth starch. *Critical Reviews in Food Science and Nutrition, 57*(2), 313–325.